

Structural and Biochemical Characterization of AidC, a Quorum-Quenching Lactonase with Atypical Selectivity

Romila Mascarenhas,[§] Pei W. Thomas,[†] Chun-Xiang Wu,^{||} Boguslaw P. Nocek,[⊥] Quyen Q. Hoang,^{||} Dali Liu,^{*,§} and Walter Fast^{*,†,‡}

[†]Medicinal Chemistry Division, College of Pharmacy, and [‡]Center for Infectious Disease, The University of Texas, Austin, Texas 78712, United States

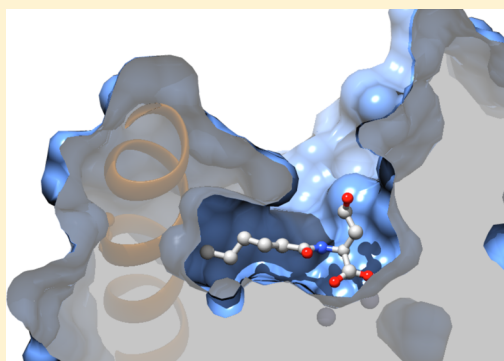
[§]Department of Chemistry and Biochemistry, Loyola University Chicago, Chicago, Illinois 60660, United States

^{||}Department of Biochemistry and Molecular Biology, Indiana University School of Medicine, Indianapolis, Indiana 46202, United States

[⊥]Structural Biology Center, Biosciences Division, Argonne National Laboratory, Argonne, Illinois 60439, United States

S Supporting Information

ABSTRACT: Quorum-quenching catalysts are of interest for potential application as biochemical tools for interrogating interbacterial communication pathways, as antibiofouling agents, and as anti-infective agents in plants and animals. Herein, the structure and function of AidC, an *N*-acyl-L-homoserine lactone (AHL) lactonase from *Chryseobacterium*, is characterized. Steady-state kinetics show that zinc-supplemented AidC is the most efficient wild-type quorum-quenching enzymes characterized to date, with a k_{cat}/K_M value of approximately $2 \times 10^6 \text{ M}^{-1} \text{ s}^{-1}$ for *N*-heptanoyl-L-homoserine lactone. The enzyme has stricter substrate selectivity and significantly lower K_M values (ca. 50 μM for preferred substrates) compared to those of typical AHL lactonases (ca. >1 mM). X-ray crystal structures of AidC alone and with the product *N*-hexanoyl-L-homoserine were determined at resolutions of 1.09 and 1.67 Å, respectively. Each structure displays as a dimer, and dimeric oligomerization was also observed in solution by size-exclusion chromatography coupled with multiangle light scattering. The structures reveal two atypical features as compared to previously characterized AHL lactonases: a “kinked” α -helix that forms part of a closed binding pocket that provides affinity and enforces selectivity for AHL substrates and an active-site His substitution that is usually found in a homologous family of phosphodiesterases. Implications for the catalytic mechanism of AHL lactonases are discussed.



One of the most prominent social behaviors displayed by bacteria is quorum sensing, the ability to coordinate gene expression in response to population density through the production and detection of interbacterial signaling molecules such as the *N*-acyl-L-homoserine lactones (AHLs).¹ Enzymes capable of blocking these signaling pathways, called quorum-quenching enzymes, are important biochemical tools for probing quorum-sensing pathways.² They also hold considerable promise as reagents for preventing marine and membrane biofouling, as treatments to prevent costly infections of plants and fish, as potential protein therapeutics, and possibly as tools to manipulate interactions between diverse microbes.^{3–7} Some of the quorum-quenching enzymes most widely used for such applications are AHL lactonases, which use a dinuclear zinc center to hydrolyze a wide range of AHL substrates (Figure 1).⁸

The gene encoding an AHL lactonase with unusual properties has been previously identified, *aidC*, an autoinducer degrading gene isolated from *Chryseobacterium* sp. strain StRB126 originally associated with potato roots.⁹ The encoded

protein, AidC (GenBank entry BAM28988, EC 3.1.1.81), catalyzes the hydrolytic ring opening of multiple *N*-acyl homoserine lactone (AHL) substrates. Analysis of protein sequence alignments revealed that AidC is homologous to other AHL lactonases found in the metallo-hydrolase/oxidoreductase superfamily and shares a conserved dinuclear metal binding motif. However, AidC is phylogenetically distant from the other AHL lactonase clusters.⁹ For example, optimal global pairwise alignment¹⁰ of AidC with two other homologous dizinc AHL lactonases, AiiA (autoinducer inactivator A from *Bacillus* sp. 240B1¹¹) and AiiB (autoinducer inactivator B from *Agrobacterium tumefaciens* C58¹²), shows only ~20 and ~17% amino acid identity, respectively. Additionally, these sequence alignments predict that active-site Asp and Tyr residues, conserved in other AHL lactonases because of their roles in zinc binding and catalytic turnover, are

Received: May 6, 2015

Revised: June 25, 2015

Published: June 26, 2015



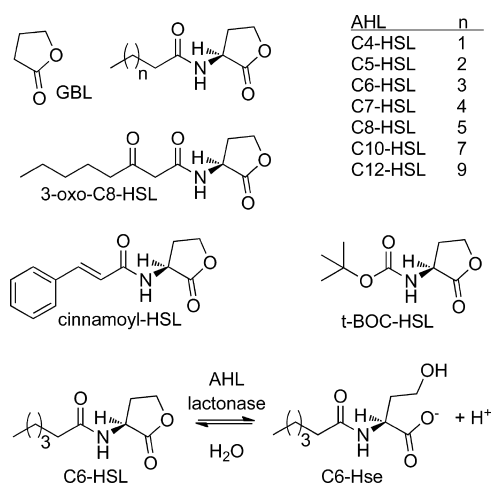


Figure 1. Potential substrates and the AHL lactonase-catalyzed reaction. γ -Butyrolactone (GBL) and naturally occurring and synthetic AHLs, including C4-, C5-, C6-, C7-, C8-, 3-oxo-C8-, C10-, C12-, cinnamoyl-, and *t*-BOC-HSL, are assayed as potential AidC substrates. The inset table assigns chain lengths in the neighboring structures to the matching abbreviations used throughout the text. The general reaction catalyzed by AHL lactonases is also shown with C6-HSL as an example, resulting in the C6-Hse and H^+ products.

possibly replaced in AidC by Leu and Ser, respectively.^{9,13,14} However, the most striking feature of AidC is its reported K_M values. All previously characterized wild-type AHL lactonases have K_M values of ≥ 1.4 mM,^{14–16} with the exception of MomL (440 μ M; *Muricauda olearia* marine AHL lactonase).¹⁷ In contrast, the reported K_M values for AidC are approximately ≥ 24 -fold lower (46–72 μ M).⁹ The lower K_M values of AidC are of interest because a better understanding of how quorum-quenching enzymes recognize and process their substrates can allow their appropriate selection and optimization as biochemical tools and help in the proposed development of this class of enzymes as therapeutic, anti-infective, and antibiofouling proteins.^{3–7} Toward these ends, we report here the characterization of purified AidC alone and with a bound product. Two aspects of the active site are atypical compared to those of previously characterized AHL lactonases: a novel substrate binding pocket defined, in part, by an unusual “kinked” α -helix containing an internal proline residue and an active-site His substitution that is usually found in more distant superfamily members that belong to a different family, the phosphodiester hydrolases.

MATERIALS AND METHODS

Materials. Unless otherwise noted, all chemicals were purchased from Sigma-Aldrich Chemical Co. (St. Louis, MO), and all enzymes used for cloning were purchased from New England BioLabs (Beverly, MA). The lactones assayed as substrates, γ -butyrolactone (GBL) and *tert*-butyl(tetrahydro-2-oxo-3-furanyl)carbamate (*t*-BOC-HSL), were purchased from Sigma-Aldrich Chemical Co. *N*-Butyryl-*L*-homoserine lactone (C4-HSL) and *N*-3-oxo-octanoyl-*L*-homoserine lactone (3-oxo-C8-HSL) were from Cayman Chemical Co. (Ann Arbor, MI). *N*-Pentanoyl-*(S)*-homoserine lactone (C5-HSL), *N*-hexanoyl-*(S)*-homoserine lactone (C6-HSL), *N*-heptanoyl-*(S)*-homoserine lactone (C7-HSL), *N*-octanoyl-*(S)*-homoserine lactone (C8-HSL), *N*-decanoyl-*(S)*-homoserine lactone (C10-HSL), *N*-dodecanoyl-*(S)*-homoserine lactone (C12-HSL), and *N*-cinnamoyl-*(S)*-HSL (C-HSL) were synthesized from *(S)*- α -

amino- γ -butyrolactone hydrochloride and the corresponding acyl chloride using methods similar to those described previously.^{14,18} Substrate stock solutions were prepared in methanol, with the final assay mixtures containing 1% methanol cosolvent.

Cloning, Expression, and Purification of AidC. The coding sequence for AidC from *Chryseobacterium* sp. strain StrB126 was codon optimized for expression in *Escherichia coli*. A sequence encoding the cleavage site for tobacco etch virus (TEV) protease (ENLYFQG) was inserted at the 5' end of the AidC coding region. Restriction sites *Eco*RI and *Not*I were added to the 5' and 3' ends, respectively, and the resulting sequence was ordered from Integrated DNA Technologies, Inc. (Figure S1 of the Supporting Information). A shuttle vector carrying the synthesized gene and a commercial protein expression vector, pMAL-C5X (New England Biolabs), were both digested using restriction enzymes *Eco*RI and *Not*I, and the resulting insert containing *aidC* was ligated into the expression vector using T4 DNA Ligase (New England Biolabs) to yield a protein expression plasmid encoding an N-terminal maltose binding protein (MBP) linked through a TEV cleavage sequence to the full length AidC enzyme. The resulting vector (pMAL-t-AidC) was used to transform *E. coli* DH5 α cells for plasmid storage and amplification. The entire coding region in pMAL-t-AidC was verified by DNA sequencing to determine that there were no unintended mutations (CRC DNA Sequencing, University of Chicago, Chicago, IL).

For protein production and purification, pMAL-t-AidC was used to transform *E. coli* BL21(DE3) cells. The resulting *E. coli* BL21(DE3)(pMAL-t-AidC) cells were incubated at 37 °C while being shaken in Luria-Bertani (LB) medium supplemented with 100 μ g/mL ampicillin. When the culture OD₆₀₀ value reached 0.6–0.8 absorbance unit, expression of the MBP-t-AidC fusion protein was induced by addition of 0.3 mM isopropyl β -D-1-thiogalactopyranoside. The LB medium was supplemented with 0.5 mM ZnSO₄, and expression was continued for an additional 16–18 h at 25 °C after induction. Cells were harvested by centrifugation at 12400g, washed with wash buffer [20 mM Tris-HCl buffer with 200 mM NaCl (pH 7.4)], and stored at –80 °C after being flash-frozen in liquid nitrogen. The frozen cell pellet was thawed, sonicated in wash buffer, and centrifuged at 40000g to pellet cell debris, which was discarded. The resulting supernatant was loaded onto an amylose affinity column (16 mm \times 25 mm Dextrin Sepharose-MBL Trap HP, GE LifeSciences, preequilibrated with wash buffer). The column was washed with wash buffer, and the MBP-t-AidC fusion protein was eluted from the column using wash buffer supplemented with maltose (10 mM). Fractions were evaluated using Coomassie-stained sodium dodecyl sulfate–polyacrylamide gel electrophoresis (SDS–PAGE), and those fractions containing MBP-t-AidC were combined and treated batchwise with TEV protease, following previously published protocols.¹⁹ The resulting cleaved proteins were exchanged into ion exchange buffer [20 mM Tris-HCl and 5 mM NaCl (pH 7.5)] and loaded onto a column (XK 16/20 GE LifeSciences) loaded with diethylaminoethanol (DEAE)-sepharose ion exchange resin to separate MBP, TEV protease, and the untagged AidC. The column was equilibrated with ion exchange buffer [20 mM Tris-HCl and 5 mM NaCl (pH 7.5)], and after loading, the protein was eluted with a linear gradient between ion exchange buffer and the same buffer supplemented by 1 M NaCl. Fractions containing untagged AidC protein were

pooled, concentrated using a 10000 molecular weight cutoff (MWCO) Amicon-Ultra centrifugal filter device (Millipore), and further purified by size-exclusion chromatography using a HiLoad Superdex-200PG column (16 mm × 600 mm, GE Lifesciences). The column was equilibrated and the protein purified using size-exclusion buffer [50 mM HEPES buffer and 300 mM NaCl (pH 7.5)]. During the purification, fractions were assayed for the presence of MBP-*t*-AidC or AidC at each step by using 12% SDS-PAGE, followed by staining with EX-Run Gel Staining Solution (Fisher BioReagents) to detect bands at ~75 or ~32 kDa, respectively. The final purified untagged AidC protein appeared to be homogeneous when characterized on a Coomassie-stained 12% SDS-PAGE gel. Protein concentrations in solution were measured using bovine serum albumin (BSA) standards and the Bradford assay (Bio-Rad). This purification procedure typically results in a yield of 10 mg of purified untagged AidC/L of culture medium.

Determining the Zinc Dependence, Steady-State Kinetic Parameters, and Zinc Content of Purified AidC.

Substrate hydrolysis rates were monitored using a previously described continuous spectrophotometric assay in which the pH indicator phenol red acts as part of the assay buffer [1 mM Hepes (pH 7.5)], which results in a change in the colorimetric signal upon protonation by the net release of a proton upon lactone hydrolysis.¹⁹ The optimal assay buffer zinc concentration was determined by monitoring hydrolysis of saturating concentrations of C6-HSL (1 mM) as catalyzed by AidC (27 nM) to determine the maximal observed initial rates with a variation in the zinc concentration (0–100 μM). To determine the relationship between AidC concentration and k_{cat} , the substrate *t*-BOC-HSL (5 mM) was used at saturating concentrations while the enzyme concentration was varied (0–250 nM). The concentration of AidC was determined using a calculated²⁰ extinction coefficient ($\epsilon_{280} = 29160 \text{ M}^{-1} \text{ cm}^{-1}$). The stoichiometry of bound zinc ions to protein in purified AidC was determined by dividing the total zinc concentration determined using the colorimetric chelator 4-(2-pyridylazo)-resorcinol under denaturing conditions, as described previously,²¹ by the concentration of AidC.

Crystallization. Purified AidC was concentrated to 20 mg/mL using a 10000 molecular weight cutoff (MWCO) Amicon-Ultra centrifugal filter device (Millipore), and the concentrated protein was buffer exchanged into crystallization screening buffer [50 mM HEPES (pH 7.0)]. Crystallization screens (Crystal Screen 1 and 2, Crystal Screen Cryo 1 and 2, PEG Ion 1 and 2, and Index 1 and 2 from Hampton Research and Wizard 1 and 2 from Emerald BioSystems) were prepared using a Crystal Gryphon (ArtRobbins) crystallization robot using a 1:1 well solution:AidC stock solution (20 mg/mL) ratio. Crystals appeared in the well solution containing $\text{MgCl}_2 \cdot 6\text{H}_2\text{O}$ (0.2 M), Bis-Tris (0.1 M) (pH 6.5), and 25% (w/v) PEG 3350 after a week upon incubation at room temperature. Crystallization was repeated and optimized using a 1:2 well solution:AidC (20 mg/mL) ratio in sitting drops, and crystals were seeded on day 3 with AidC crystals obtained from previous trials. Crystallization was conducted in 24-well Cryschem Plates (Hampton Research). For cocrystallization of AidC and substrate, 4 μL of AidC (20 mg/mL) was mixed with 1 μL of well solution and 1 μL of 10 mM C6-HSL (dissolved in 50% methanol). Crystals formed within a week of seeding, during which C6-HSL likely hydrolyzed to the ring-opened product *N*-hexanoyl-L-homoserine (C6-Hse). AidC and AidC:C6-Hse crystals with the best morphology were trans-

ferred into a cryoprotecting solution [well solution supplemented with 25% (v/v) glycerol] and then into liquid nitrogen.

Data Collection and Processing. Monochromatic data sets were collected at the 19-BM beamline at the Structural Biology Center (SBC), Advanced Photon Source (APS), at Argonne National Laboratory (ANL). Diffraction data were collected at a wavelength of 0.98 Å at 100 K using a Quantum 210r Charge Coupled Device (CCD) detector from Area Detector Systems Corp. (ADSC). All collected data sets were indexed and integrated using iMosflm²² and scaled using Scala in the CCP4 program suite.²³ The best data sets were processed at resolutions of 1.09 and 1.67 Å for AidC and AidC:C6Hse, respectively. Data collection statistics are summarized in Table 1.

Structure Determination, Model Building, and Refinement. The AidC structure was determined by molecular replacement using PHASER in the Phenix software suite.²⁴ The initial search model was a polyaniline model created on the basis of a previously published structure of the organic

Table 1. Crystallographic Data for AidC and AidC:C6-Hse Complexes

	AidC	AidC:C6-Hse
Protein Data Bank entry	4ZO2	4ZO3
Data Processing		
space group	$P2_12_12_1$	$P2_12_12_1$
cell dimensions		
α, β, γ (deg)	90, 90, 90	90, 90, 90
a, b, c (Å)	51.7, 97.30, 110.64	47.09, 47.87, 249.15
resolution (Å)	1.09	1.67
R_{merge}^a (%)	4.9 (100) ^b	9.3 (75.4)
$I/\sigma(I)$	23.6 (1.1)	20.3 (3.3)
$\text{CC}_{1/2}^c$	0.997 (0.539)	0.992 (0.767)
R_{pim}^d (%)	3.00 (60.8)	5.0 (41.8)
completeness (%)	99.6 (99.2)	99.3 (99.9)
multiplicity	6.6 (3.4)	4.4 (3.9)
no. of reflections	1580815	295571
no. of unique reflections	239792	67109
Refinement		
average B factor (Å ²)	23.6	28.8
$R_{\text{work}}^e/R_{\text{free}}^f$ (%)	13.08/16.20	18.44/22.83
no. of atoms		
protein	4810	4714
ligand	N/A ^h	30
metal	4	4
water	955	585
B factor		
protein	21.5	27.4
ligand	N/A ^h	32.69–47.58
rmsd ^g		
bond lengths (Å)	0.015	0.018
bond angles (deg)	1.401	1.164
Ramachandran plot (%)		
most favored	97.70	97.29
allowed	2.20	2.54
outliers	0.00	0.17

^a $R_{\text{merge}} = \sum |I_{\text{obs}} - I_{\text{avg}}| / \sum I_{\text{avg}}$. ^bThe values for the highest-resolution bin are in parentheses. ^cPearson correlation coefficient of two “half” data sets. ^dPrecision-indicating merging R . ^e $R_{\text{work}} = \sum |F_{\text{obs}} - F_{\text{calc}}| / \sum F_{\text{obs}}$. ^fFive percent of the reflection data were selected at random as a test set, and only these data were used to calculate R_{free} . ^gRoot-mean-square deviation. ^hNot applicable.

phosphotriesterase OPHC2 [Protein Data Bank (PDB) entry 4LE6, organophosphate hydrolase C2 from *Pseudomonas pseudoalcaligenes*],²⁵ because this enzyme shares 26% amino acid sequence identity with AidC. The program Phenix.Auto-build was used to build the residue side chains based on the phases obtained from running PHASER; Phenix.Auto-build uses iterative cycles of model building and refinement until no more side chains can be built in automatically.²⁴ The AidC:C6Hse structure was determined by molecular replacement using PHASER in the CCP4 software suite; the search model was the unliganded AidC structure.²⁶ Both models were rebuilt and refined using the program Phenix²⁴ and analyzed using COOT²⁷ and UCSF Chimera.²⁸ Final refinement statistics are listed in Table 1. Structural figures were made using UCSF Chimera.

Determining Oligomeric States of AidC and AiiA. To determine the molecular mass of AidC oligomers in solution, we used size-exclusion chromatography coupled with multi-angle light scattering (SEC-MALS). Our experimental setup included an AKTA FPLC system (GE Healthcare Biosciences) with a silica-based size-exclusion chromatography column (WTC-030S5, Wyatt Technology) as a liquid chromatography unit. Downstream of the column is a refractive index detector (Optilab T-REX, Wyatt Technology), followed by a multiangle light scattering detector (Dawn Heleos II, Wyatt Technology) used for determining protein concentration and particle size, respectively. As a control sample, we analyzed the related AHL lactonase AiiA, which is of similar monomeric size and has previously been demonstrated by analytical ultracentrifugation to be a monomer in solution.²⁹ Each sample injection consisted of approximately 0.5–1 mg (injection volume of 95 μ L) of purified protein (either AiiA or AidC) in a buffer containing 50 mM HEPES and 300 mM NaCl (pH 7.5). The flow rate was set at 0.4 mL/min, and data were collected at 2 s intervals. Data processing and analysis were performed using the ASTRA software (Wyatt Technology).

RESULTS AND DISCUSSION

Most AHL lactonases characterized to date have poor affinity for their substrates, as gauged by millimolar K_M values. However, unusually low micromolar K_M values were reported for AidC-catalyzed hydrolysis of AHLs.⁹ To better understand the basis for substrate affinity, selectivity, and turnover in AidC, we cloned and purified this AHL lactonase for functional and structural studies.

Purification of AidC and Determination of Activity and Zinc Content. Heterologous expression of AidC in *E. coli* using a codon-optimized coding sequence (Figure S1 of the Supporting Information) led to good yields of purified protein (~10 mg/L of culture). Kinetic characterization of the “as purified” form of untagged AidC gave K_M ($65 \pm 4 \mu$ M) and k_{cat} ($4.6 \pm 0.1 \text{ s}^{-1}$) values for lactone hydrolysis of C6-HSL similar to values reported previously for AidC containing an N-terminal maltose binding protein affinity tag ($55 \pm 4 \mu$ M and $2.3 \pm 0.2 \text{ s}^{-1}$, respectively).⁹ Although we used a purification procedure similar to that for other AHL lactonases,¹⁹ we found that purified AidC does not contain the typical 2 equiv of zinc ions. Instead, the “as purified” AidC preparation contained only 1.2 ± 0.1 equiv of zinc ions per AidC monomer. We suspected that the protein may not have fully retained its zinc content throughout the purification protocol and so monitored the observed rates for AidC-mediated hydrolysis of saturating concentrations of substrate upon supplementing the assay

buffer with varying concentrations of ZnSO_4 (Figure 2). A significant increase in rate is observed with an increase in

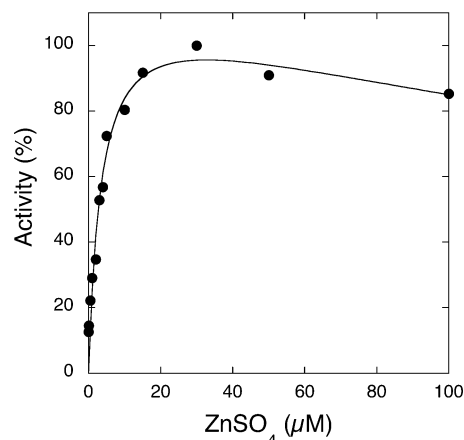


Figure 2. Optimization of the assay zinc concentration. The relative observed initial rates of AidC-catalyzed hydrolysis of C6-HSL under saturating conditions (1 mM) are graphed with respect to the concentrations of supplemental ZnSO_4 added to assay buffer. Maximal activity was detected at 30 μ M supplemental ZnSO_4 . Points are fitted to the equation $\text{activity (\%)} = \text{Act}_{\text{max}} \times [\text{Zn}^{2+}] / [\text{EC}_{50} + [\text{Zn}^{2+}](1 + [\text{Zn}^{2+}]/K_i)]$, where Act_{max} is the maximal activity, EC_{50} is the half-maximal concentration of activation, and K_i is the apparent inhibition constant, with fitted values of $120 \pm 10\%$, $3.6 \pm 0.9 \mu$ M, and $300 \pm 180 \mu$ M, respectively.

ZnSO_4 concentration, with a maximal activity at approximately 30 μ M ZnSO_4 , and a slight decrease at higher concentrations. Zinc supplementation leads to an increased k_{cat} (C6-HSL, $59 \pm 1 \text{ s}^{-1}$), which is >10-fold larger than the k_{cat} of the “as purified” form. If the 1.2 equiv of zinc ions in the “as purified” AidC represents approximately half dizinc protein and half zinc-free protein, one might expect a 2-fold increase in k_{cat} values, at most, upon reconstitution of the dizinc active site. However, because the observed increase in rate is much larger, it likely represents instead an increase in activity due to the transition between mono- and dizinc metalloforms. Further studies will be required to characterize zinc affinity in more detail. However, a supplement of 30 μ M ZnSO_4 is used for the remaining kinetic experiments herein to maximize observed activity.

Determination of Kinetic Parameters. The previous characterization of AidC containing an N-terminal maltose binding fusion protein reported unusually low K_M values (C6-HSL, 55 μ M; C8-HSL, 64 μ M), with very little selectivity for, or against, related substrates with 3-oxo substitutions.⁹ The associated k_{cat} values (approximately 2 s^{-1}) are lower than those typically reported for AHL lactonases. To augment this previous study, we determined the steady-state kinetic parameters for purified, untagged AidC, now supplemented with exogenous ZnSO_4 , using a broader set of substrates (Table 2). In general, we confirm the low K_M values reported previously. The K_M values for zinc-supplemented AidC, “as purified” AidC, and AidC with an N-terminal maltose binding fusion protein are all quite similar, independent of zinc content. However, zinc supplementation (but not cleavage of the N-terminal tag) greatly improves the k_{cat} values, which are all generally increased by >20-fold. These results indicate that the differences in k_{cat} values between this and the prior report likely arise from differences in zinc content rather than the presence of the N-terminal fusion protein.

Table 2. Steady-State Kinetic Parameters for Substrates of Dizinc AidC

substrate	K_M (μM)	k_{cat} (s^{-1})	k_{cat}/K_M ($\text{M}^{-1} \text{s}^{-1}$)
GBL	ND ^a	ND ^a	16 ± 1
C4-HSL	470 ± 60	39 ± 2	8.3×10^4
C5-HSL	130 ± 20	57 ± 3	4.4×10^5
C6-HSL	61 ± 4	59 ± 1	9.7×10^5
C7-HSL	47 ± 5	80 ± 2	1.7×10^6
C8-HSL	83 ± 10	45 ± 3	5.4×10^5
C10-HSL	12 ± 4	5.2 ± 0.4	4.3×10^5
C12-HSL	7 ± 4	0.40 ± 0.05	5.7×10^4
3-oxo-C8-HSL	130 ± 20	28 ± 1	2.2×10^5
cinnamoyl-HSL	470 ± 80	25 ± 2	5.3×10^4
<i>t</i> -BOC-HSL	740 ± 70	44 ± 1	5.9×10^4

^aNot determined. The K_M value for GBL exceeds 700 mM, so only the k_{cat}/K_M value was determined.

As compared to other quorum-quenching enzymes, AidC appears to be a much more efficient catalyst. If the k_{cat}/K_M value for hydrolysis of the best AHL substrate of AidC is compared with k_{cat}/K_M values for the best of the kinetically characterized substrates for other wild-type quorum-quenching enzymes (including nonhomologous enzymes from different superfamilies), AidC ranks the highest (Table 3). Achieving the

Table 3. Steady-State Rate Constants for Selected Wild-Type Quorum-Quenching Enzymes and AHL Substrates with the Highest Reported k_{cat}/K_M Values

enzyme	substrate	k_{cat} (s^{-1})	K_M (μM)	k_{cat}/K_M ($\text{M}^{-1} \text{s}^{-1}$)	ref
AidC	C7-HSL	80	47	10^6	this work
MomL	3-oxo-C10-HSL	224	440	10^5	17
PvdQ ^a	C12-HSL	2.5	11	10^5	50
PON2 ^b	3-oxo-C12-HSL	13	50	10^5	48
PONX_OCCAL ^c	3-oxo-C12-HSL	44	180	10^5	48
AiiA	C6-HSL	91	5600	10^4	14
AiiB	C6-HSL	25	1600	10^4	16
MCP ^d	C12-HSL	0.3	23	10^4	51
VmoLac ^e	C8-HSL	0.6	260	10^3	52
GKL ^f	C8-HSL	0.5	1200	430	53

^aPyoverdine biosynthetic protein Q from *Pseudomonas aeruginosa*. The enzyme belongs to the metal-independent NTN-hydrolase superfamily. ^bParaoxonase-2 from human. The enzyme belongs to the dicalcium binding paraoxonase family with a six-bladed β -propeller fold. ^cParaoxonase X from *Oceanicaulis alexandrii*. The enzyme belongs to the same family as PON-2. ^dLactonase from *Mycobacterium avium* subsp. *paratuberculosis* K-10. The enzyme belongs to the phosphotriesterase-like lactonase group of enzymes within the amidohydrolase superfamily. ^eLactonase from the hyperthermophile *Vulcanisaeta moutnovskia*. The enzyme belongs to the same group as MCP. ^fLactonase from the thermophile *Geobacillus kaustophilus*. The enzyme belongs to the same group as MCP.

highest rank in this comparison is due to a combination of both a low K_M value and a high k_{cat} value, because AidC does not have the lowest or highest of either of these individual values with respect to the same set of enzyme/substrate pairs (Table 3). Therefore, to the best of our knowledge, AidC appears to have the highest k_{cat}/K_M reported for any wild-type quorum-

quenching enzyme to date. Additionally, even when k_{cat}/K_M values are similar, the low K_M value of AidC may make this enzyme more suitable than homologues with higher K_M values for quorum-quenching applications at low AHL concentrations.³⁰

Substrate Selectivity. As gauged by k_{cat}/K_M values, the most efficiently processed substrates of AidC are C6- and C7-HSL ($\sim 10^6 \text{ M}^{-1} \text{ s}^{-1}$) (Table 2). AHL substrates that differ in length by one methylene have a >2-fold decrease in their specificity constant (k_{cat}/K_M). Commonly occurring AHLs with more extreme size differences, C4- and C12-HSL, are more significantly disfavored by 20- and 30-fold, respectively. The previous characterization of AidC indicated no preference for or against 3-oxo substitutions,⁹ and here we find consistent results in which the 3-oxo substitution only mildly perturbs both K_M and k_{cat} values, resulting in a 2.5-fold decrease in k_{cat}/K_M . The most significantly disfavored substrates we assayed were the bulky cinnamoyl-HSL³¹ and the synthetic *t*-BOC-HSL compound, which had specificity constants approximately 30-fold lower than that of the best substrate. Interestingly, the mechanism used to disfavor substrates with sterically bulky substituents appears to differ from that used to disfavor substrates with long unsubstituted *n*-alkyl substituents (see below).

Structure Determination and Model Building. To better understand the structural basis of substrate recognition and catalysis, we determined the X-ray crystal structure of AidC and the structure of AidC in complex with the reaction product C6-homoserine (C6-Hse) through cocrystallization with the substrate C6-HSL. Data processing and refinement statistics are listed in Table 1. The unliganded AidC crystal diffracted to a resolution of 1.09 Å. The $2F_o - F_c$ omit map for the active-site zinc ions and coordinating residues is shown in Figure 3. The

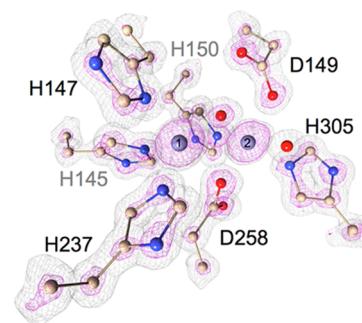


Figure 3. $2F_o - F_c$ omit map for the unliganded AidC dizinc site and coordinating residues. The map is shown at two different σ levels, with the gray mesh at 1.5σ and the magenta mesh at 4.0σ . The protein and zinc atoms are shown in ball-and-stick form, and colored as follows: tan for carbon, blue for nitrogen, red for oxygen, and gray for zinc. The 4σ map can be seen to indicate individual atom positions, characteristic of an ultra-high-resolution map.

“substrate-treated” AidC cocrystal diffracted to a resolution of 1.67 Å and contained the ring-opened product, C6-Hse. The final R_{work} and R_{free} values are 13.08 and 16.20% for AidC and 18.44 and 22.83% for AidC:C6-Hse, respectively. The occupancies of the zinc ions are refined to values between 0.6 and 0.8, as assessed by occupancy refinement in Phenix. During crystallization, the concentration of the enzyme is higher and the solution pH values are lower than during the functional studies discussed above. Therefore, these occupancies may not

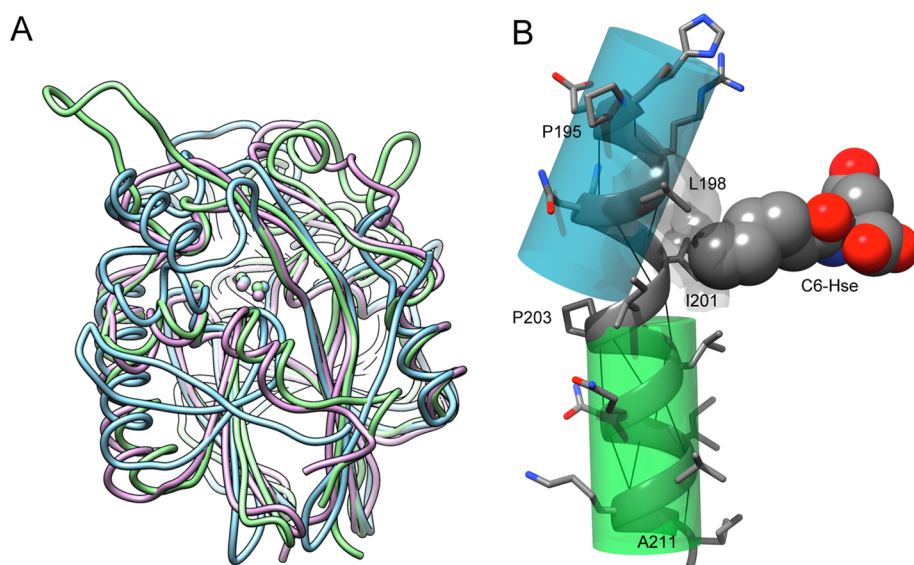


Figure 4. Structure of the AidC monomer. (A) Superimposition of AidC (blue), AiiA (pink), and AiiB (green) structural models. Proteins backbones are depicted as “licorice” strands. The level of structural conservation is higher in the zinc binding site and the $\alpha\beta\alpha$ core scaffold of the protein but diverges more significantly in the connecting elements surrounding the active site. (B) Ribbon diagram of a “kinked” α -helix in AidC containing an internal proline residue. The regular H-bonding pattern (thin black lines) of the α -helix backbone from residue P195 to A211 is interrupted by an internal P203 residue. The two ends of the α -helix, defined as P195–Q200 (blue) and A204–A211 (green), are offset by approximately 25°. Hydrophobic side chains near the bend, I201 and L198 (surface colored gray), contribute to the binding site for the N-acyl substituent of the bound product (C6-Hse, shown in space-fill form).

reflect zinc binding during kinetic studies and will be a topic for future experiments.

AidC Core Structure, “Kinked” Helix, and Dimerization. The AidC monomer structure displays a characteristic pseudosymmetrical core of two mixed β -sheets flanked by α -helices to form the $\alpha\beta\alpha$ protein fold conserved throughout the entire metallo-hydrolase/oxidoreductase superfamily, as cataloged in the Structural Classifications of Proteins (SCOP) database.³² A dinuclear zinc ion cluster is found at one edge of where the two central β -sheets meet and is described below in more detail as part of the active site. A structural overlay of AidC with two related AHL lactonases, AiiA²⁹ and AiiB,¹⁶ highlights their conserved $\alpha\beta\alpha$ cores and shows the most significant structural divergence occurs in loops and helices, adjacent to the dizinc active site, which serve to connect the core secondary structural elements (Figure 4A). Parts of these regions interact closely with active-site ligands.

The AidC structure contains an unusual feature. One of the major helices, H11 (see Figure S2 of the Supporting Information for secondary structure assignments), containing residues P195–A211 has an internal proline residue (P203) that disrupts the regular H-bonding of the α -helix. It results in a “kinked” structure in which one segment of the α -helix is found at an approximate 25° angle from the other (Figure 4B). Most soluble proteins do not contain α -helices with internal proline residues, but this feature is not unprecedented.³³ A survey of 291 helices found that approximately 3% contain an internal proline, and the associated helix “kinks” typically measure $26 \pm 5^\circ$, tilting away from the proline side chain, consistent with what is found in AidC.³⁴ Kinked α -helices typically place the hydrophobic side chain of the internal proline residue toward the solvent, and the kink aids in packing long helices around globular proteins;³⁵ both of these attributes are observed in AidC. Proline residues responsible for inducing kinks are typically highly conserved,³⁴ but P203 is not a conserved residue in this superfamily. However, several side chains of

residues near the P203-induced kink do form part of the AidC substrate binding cavity, suggesting a functional implication for this unusual structural element.

In our structural determination, AidC displays as a crystallographic dimer in space group $P2_12_12_1$ (Figure 5A). The protein–protein interface is heterogeneous and comprised of hydrophobic interactions as well as direct and through-water hydrogen bonds. The Proteins Interfaces Structures and Assemblies (PISA) algorithm³⁶ was used to calculate a buried surface area of 2440 Å² and predicts a ΔG^{diss} of 6.1 kcal/mol. To determine if oligomerization is relevant in solution, SEC–MALS was used to assay AidC oligomers (Figure 6). First, AiiA was used as a control because this homologous AHL lactonase was previously shown by analytical ultracentrifugation to be monomeric in solution.²⁹ Purified AiiA elutes from the size-exclusion column as a single peak (detected by Abs₂₈₀), and light scattering is used to determine a molecular weight of 28 ± 2 kDa for this peak, which matches the mass calculated from the expected sequence (28635 Da). Purified AidC elutes from the size-exclusion column as one major peak preceded by a small second peak. The molecular weight determined for the major peak, 72.1 ± 0.9 kDa, matches reasonably well with that calculated for the dimer ($36979 \text{ kDa} \times 2 = 73958 \text{ kDa}$). The molecular weight calculated for AidC oligomers in the small minor peak is 148 ± 4 kDa, which matches that calculated for the tetramer ($36979 \text{ kDa} \times 4 = 147916 \text{ kDa}$). Therefore, at least when high protein concentrations are used, AidC forms a dimer in solution. Further studies will be required to determine if the dimer interface observed crystallographically is conserved in solution. Under the dilute assay conditions used to determine steady-state kinetic parameters, the activity of the enzyme varies linearly with concentration (Figure S3 of the Supporting Information). Therefore, either the dimer K_d value does not occur within the tested concentration range, or there is no change in activity with a change in oligomeric state.

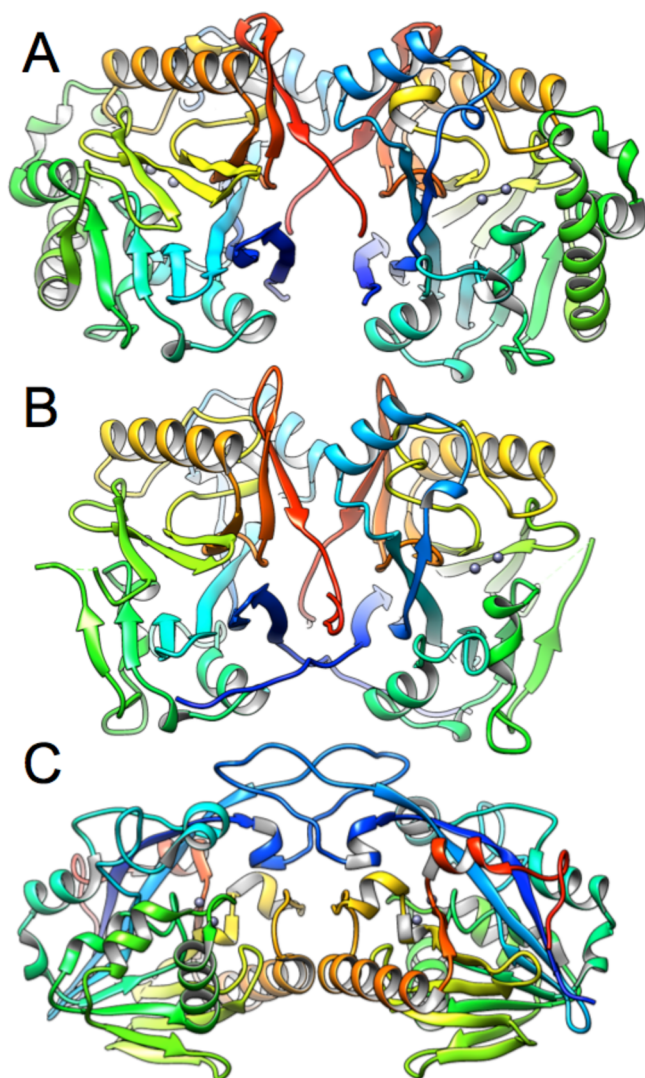


Figure 5. Dimer structure of AidC and homologues. Each monomer is shown in ribbon form, with rainbow coloring from each N-terminus (blue) to the corresponding C-terminus (red). Rainbow coloring is used here to facilitate chain tracing and to emphasize similarities and differences between the oligomeric interfaces. Zinc ions are shown as gray spheres. (A) Depiction of the AidC dimer. (B) Depiction of the OPHC2 dimer (from PDB entry 4LE6). (C) Depiction of the AiiB dimer (from PDB entry 2R2D). The dimers of AidC and OPHC2 are very similar, but that of AiiB is divergent and uses different protein–protein interfaces.

Previously, various AHL lactonases have been characterized as monomers²⁹ and dimers,¹⁶ and the superfamily has examples of higher-order oligomers. When the AidC dimer structure is compared with that of AiiB (Figure 5C), which has been observed as a dimer in a crystal,¹⁶ and in solution (unpublished observations), it is clear that the protein–protein interfaces are actually very divergent and involve different sides of the protein. However, when the AidC dimer structure is compared to the crystallographic dimer structure of the organophosphotriesterase OPHC2 (Figure 5B),²⁵ the protein–protein interfaces that comprise each dimer interface appear to be structurally conserved. In fact, the overall structural similarity of AidC ranked higher with OPHC2 than with any other AHL lactonase, as gauged by the Dali server for structural comparison of proteins.³⁷ The active sites for each AidC

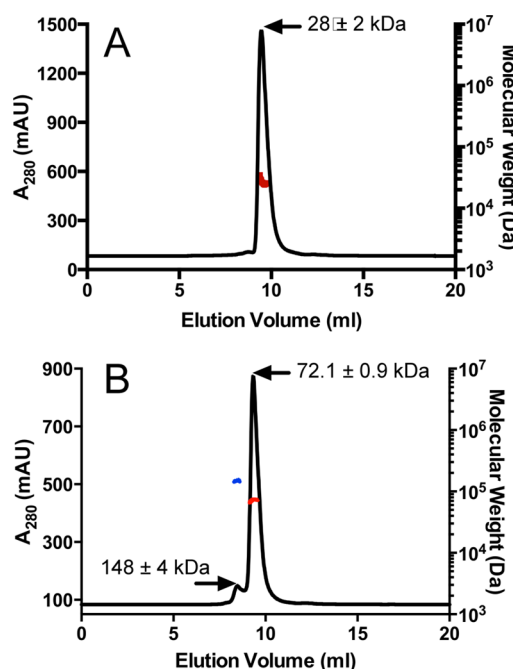


Figure 6. Molecular weight determinations of AidC and AiiA in solution. SEC–MALS profiles are shown for AiiA and AidC. The absorbance at 280 nm is shown as a black line, and the calculated molecular weight for protein in the eluent at a particular time is shown in color, as noted. (A) AiiA (molecular weight in red) gives a single peak with a molecular weight of 28 ± 2 kDa. (B). AidC gives two peaks with the major peak containing an oligomer with a molecular weight (red) of 72.1 ± 0.9 Da and a minor preceding shoulder containing an oligomer with a molecular weight (blue) of 148 ± 8 Da.

monomer are distant from each other, and none of the structural or functional evidence presented here suggests that they are interdependent. Interestingly, AidC appears also to conserve other features besides this dimerization interface, with superfamily members outside of the immediate AHL lactonase family as will be described below.

AidC Active Site. The dinuclear zinc active site of AidC is highly conserved with other AHL lactonases and other members in the superfamily. As can be seen in the comparison of dinuclear zinc sites in AidC, the AHL lactonase AiiA,²⁹ the organic phosphotriesterase OPHC2,²⁵ and the phosphodiesterase ZipD,³⁸ all the zinc-1 (Zn1) ions are coordinated by three histidines and all the zinc-2 (Zn2) ions by two histidines and an aspartate, with both zinc ions sharing a monodentate bridge by an aspartate residue and most sharing a bridging water (Figure 7). Although a bridging water is not modeled into the ZipD structure, its presence may be obscured by the resolution of the diffraction (2.9 Å). Because of its proximity to both zinc ions, this conserved bridging water is likely bound as a hydroxide ion, which is proposed to be the hydrolytic nucleophile,⁸ similar to its function in other superfamily members.³⁹ Zn1 and Zn2 of AidC also each coordinate to their own apical water molecules, illustrating the proposed coordination sites for the lactone carbonyl oxygen and ring oxygen in AHL substrates, respectively. In all cases, the Zn-to-Zn distances are all very similar (see the Figure 7 legend for relevant distances).

There is one notable difference in AidC immediately adjacent to the dinuclear zinc cluster. All of the AHL lactonases previously characterized have a Tyr [Y194 in AiiA (Figure 7B)] that we previously proposed as a H-bond donor to help

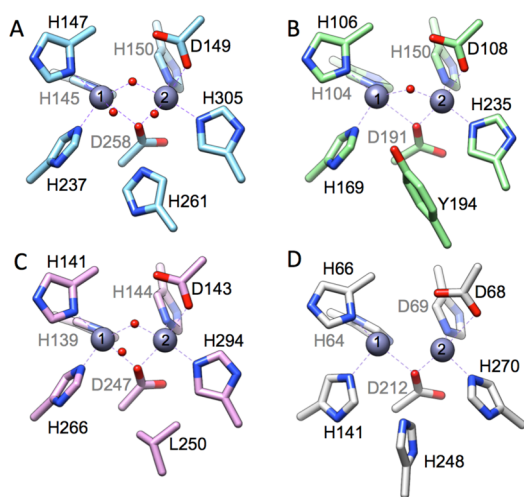


Figure 7. Unliganded active-site structures. (A) Active-site structure of AidC (blue). Protein residues are shown as sticks and zinc ions (gray) and water molecules (red) as spheres, with oxygens colored red and nitrogens blue. The Zn-to-Zn distance is 3.3 Å; the Zn–O distances to the bridging hydroxide are 1.9 and 2.0 Å. The distance from Zn1 to its apical water is 2.7 Å and that from Zn2 to its apical water 2.5 Å. The distance from the bridging hydroxide to the nonchelating O of D149 is 2.7 Å, and the distances from His261 ^N to the Zn1 and Zn2 apical waters are 3.4 and 3.0 Å, respectively. (B) Active-site structure of AiiA (green, from PDB entry 2A7M). The Zn-to-Zn distance is 3.3 Å. The Zn–O distances to the bridging hydroxide are 2.1 and 2.0 Å, and the distance from the bridging hydroxide to the nonchelating O of D108 is 2.8 Å. (C) Active-site structure of OPHC2 (pink, from PDB entry 4LE6). The Zn-to-Zn distance is 3.2 Å. The Zn–O distances to the bridging hydroxide are both 2.2 Å, and the distance from the bridging hydroxide to the nonchelating O of D143 is 2.7 Å. (D) Active-site structure of ZipD (gray, from PDB entry 2CBN). The Zn-to-Zn distance is 3.3 Å. No bridging or apical waters were modeled into the structure, possibly because of the limited diffraction resolution (2.9 Å).

stabilize a tetrahedral adduct formed in the hydrolysis reaction.⁸ However, this position in AidC is instead occupied by His261 (Figure 7A). Although the related organic phosphotriesterase OPHC2 has a Leu at this position (Figure 7C) and likely does not use this residue during catalysis, the homologous phosphodiesterase ZipD does place a His side chain in the same structural position (Figure 7D), with the residue coming from a position later in the primary sequence.

Our determination of the AidC structure allows a structural alignment to be constructed that helps to correct some prior predictions based on primary sequence alignments (Figure S4 of the Supporting Information). Leu259 was predicted to replace the zinc-bridging Asp residue,⁹ but Asp258 is seen here to retain this role. Also, Ser262 was predicted to replace the Tyr adjacent to the active site,⁹ but as discussed above, the His261 side chain is shown to occupy this position.

AidC Product Complex. Addition of the substrate C6-HSL to the crystallization mixture allowed us to characterize the interactions of the product with the AidC active site (Figure S5 of the Supporting Information). Although technically this experiment could be classified as cocrystallization, the substrate and enzyme were incubated together for 3 days before the mixture was “seeded” with unliganded AidC crystals. Therefore, this procedure may be more akin to cocrystallization with product or, if the unliganded AidC seeding biases the resulting conformation, crystal soaking with the product. Regardless, the

experiment resulted in a structure in which product was bound at the active site of AidC.

The simulated annealing omit map ($F_o - F_c$) electron density found at the active site of AidC monomer A is very well-defined and matches with that of the ring-opened product C6-Hse (Figure 8; see Figure S6 of the Supporting Information

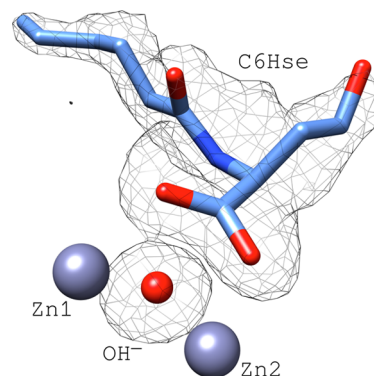


Figure 8. Simulated annealing omit map ($F_o - F_c$) for the product. The omit map is shown as a gray mesh at 2.2σ. The omit map was generated with both the C6-Hse and bridging hydroxide omitted from the coordinates. Carbon atoms are colored light blue, oxygens red, nitrogens dark blue, and zincs gray.

for the $2F_o - F_c$ omit map). The density at the same relative position in monomer B is also consistent with fitting C6-Hse but is less well-defined. The newly formed product carboxylate coordinates both zinc ions, bridging the site in a bidentate fashion (Figure 9A). The positioning of the amide and alcohol substituents is generally similar to that seen in the product complex with the homologous AHL lactonase AiiA (Figure 9B);¹³ however, there are some differences. In AidC, the product carboxylate oxygens are farther from the zinc ions (~2.5 Å) than those in product-bound AiiA (~2.1 Å). Also, the AidC product complex has a shorter Zn-to-Zn distance (3.2 Å) and retains a bridging hydroxide, but the AiiA product complex has a longer Zn-to-Zn distance (3.7 Å) and is missing the bridging hydroxide. If AidC and AiiA use the same catalytic mechanism, these two structures may represent different steps along the reaction coordinate. The AiiA structure shows that the product closely associates with the zinc ions after ring opening, and the AidC structure may illustrate how the product is then displaced by re-forming the hydroxide bridge, reducing the Zn-to-Zn distance, and lengthening the bonds between the product and the zinc ions. The product-bound AidC complex may also shed light on the relative positioning of the substrate at the active site. The bridging hydroxide is only 2.6 Å from the carbonyl carbon of the product; this close positioning may mimic the substrate-bound complex in which hydroxide attacks this substrate carbonyl. However, the ⁻OH–C4–O2 angle is only 78°, so the product is likely angled differently than substrate, for which a larger, more typical Bürgi–Dunitz angle⁴⁰ would be predicted.

One particular amino acid substitution raises the possibility that the AidC mechanism might diverge from that of AiiA. In AiiA, the Y194 residue was proposed to help stabilize the tetrahedral adduct formed upon initial hydroxide attack.¹⁴ However, the H261 residue in AidC, which occupies the same relative position, has a lower predicted pK_a value. Additionally, ^N of H261 is more distant (3.6 Å) from the product oxygen that is placed in a position that the carbonyl of the substrate is

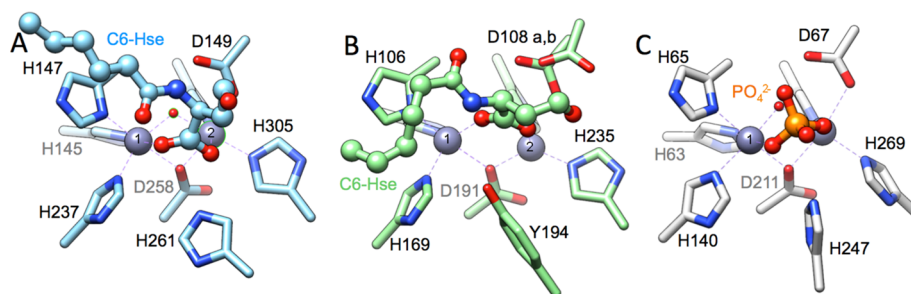


Figure 9. Product-bound active-site structures. In all cases, the liganded product is shown as balls and sticks, and the binding site consisting of protein residues is shown as sticks, with heteroatom coloring as described above. (A) Active-site structure of AidC bound to C6-Hse (blue). Measurements are given for monomer A. The Zn-to-Zn distance is 3.3 Å; the Zn–O distances to product are each 2.5 Å, and the Zn–O distances to the bridging hydroxide are each 2.0 Å. The H261 N^ε is 3.6 and 2.7 Å from the product carboxylate oxygens. (B) Active-site structure of AiiA bound to product (green, from PDB entry 3DHB). The Zn-to-Zn distance is 3.7 Å; the Zn–O distances to product are 2.0 and 2.1 Å, and the distance from the leaving group alcohol to the closest O of the unchelated conformer of D108 is 2.6 Å. The Y194 phenol O is 3.8 and 4.0 Å from the product carboxylate oxygens. (C) Active-site structure of tRNase Z bound to phosphate (gray, from PDB entry 1Y44). tRNase Z and ZipD (Figure 6D) are different proteins, but both are colored gray to indicate that they are both phosphodiesterases. The Zn-to-Zn distance is 3.3 Å. The Zn–O distances to the bridging hydroxide are 2.0 and 2.3 Å. The Zn–O distances to product are 2.3 and 2.5 Å. The distance from the closest O of D67 and PO₄^{2−} is 3.6 Å, and the other nonchelating O of PO₄^{2−} is 3.1 Å from N^ε of His247.

predicted to occupy than it is from the product oxygen that is placed in a position that the leaving group of the substrate is predicted to occupy (2.7 Å). This arrangement suggests a possible participation in ring opening through general acid/base catalysis, a mechanism reminiscent of that proposed for the homologous phosphodiesterase tRNase Z in which a structurally conserved histidine is proposed to act as a general acid during hydrolysis.⁴¹ In the phosphate-bound structure of tRNase Z, the structurally analogous histidine (His247) can be seen within H-bonding distance (3.1 Å) of one of the phosphate oxygens (Figure 9C).⁴² (Because a product-bound ZipD structure is not available, we consider instead the homologous phosphodiesterase tRNase Z, which also contains this active-site His substitution.) Further studies will be required to see if AidC uses His261 as a mimic of Y194 in AiiA or if it instead uses this residue for general acid/base catalysis or a different function.

The *N*-Alkyl Substituent Binding Pocket and a Mechanism for Selectivity. The most striking differences between the product-bound AidC and AiiA structures are the binding pockets for the *N*-acyl substituents of the products (Figure 10 and Figure S5 of the Supporting Information). AidC contains a hydrophobic pocket, formed in part by the “kinked” α -helix that completely surrounds the terminal part of the *N*-acyl substituent, which is buried below the surface of the protein (Figures 3B, 9B, and 10A). In contrast, AiiA instead cradles only the *N*-acyl substituent of C6-Hse along a wide and shallow hydrophobic trough found on the surface of the enzyme (Figure 10C,D).¹³ Products with longer *N*-acyl substituents can also bind to AiiA in an alternative orientation (not shown) in which they receive some additional stabilization by a “phenylalanine clamp”.⁴³ However, in contrast to the relatively open *N*-acyl binding site in AiiA, AidC instead contains a closed, well-defined *N*-acyl binding pocket that is unlike the substrate binding pockets in all previously characterized AHL lactonases in the superfamily, and this pocket is likely the major contributor to the uniquely low K_M values observed for substrates of this enzyme.

This binding pocket suggests a mechanism whereby AidC can impose substrate selectivity. Substrates with short *N*-acyl substituents would not be able to reach as deeply into the pocket and bury as much hydrophobic surface as longer, more

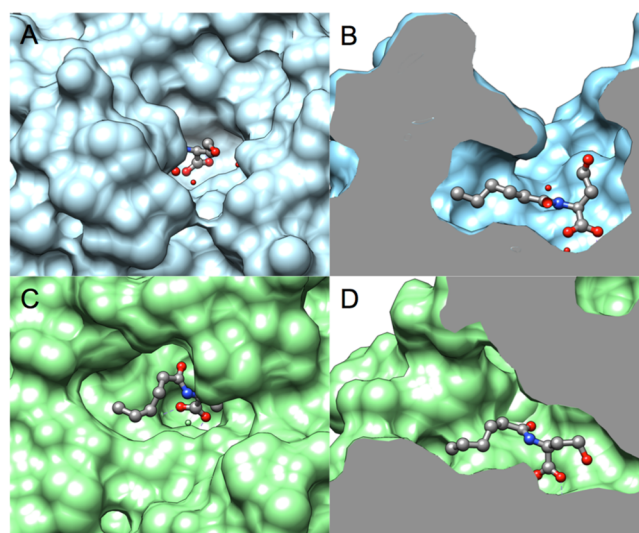


Figure 10. *N*-Acyl chain binding pockets. (A) A surface-coated AidC (blue) is shown with the C6-Hse product as balls and sticks (carbons colored gray and heteroatoms as described above). The *N*-acyl chain of the product is buried below the surface. (B) A rotated, cut-away view of panel A, showing a defined pocket for binding the *N*-acyl chain of the product, while the opened ring is pointing toward the solvent. (C) A surface-coated AiiA (green, from PDB entry 3DHB) is shown with the C6-Hse product as balls and sticks (coloring as described above). The *N*-acyl chain lies in a shallow groove of the enzyme and is visible from the surface. (D) A rotated, cut-away view of panel C, showing the *N*-acyl chain of the product extending toward the solvent and the opened ring enclosed in a more defined pocket.

favorable substrates, and a resulting difference in K_M values would ensue. For example, C4-HSL has a K_M value 10-fold higher than that of C7-HSL, but the differences in k_{cat} values are more minor. The same effect is seen with substrates containing very bulky *N*-acyl substituents that can not easily enter the buried pocket, such as cinnamoyl- and *t*-BOC-HSL, which have K_M values 10- and 16-fold higher than that of C7-HSL, respectively, again with weaker effects on k_{cat} values. In contrast, substrates with longer *N*-acyl substituents would be disfavored by a different mechanism. The long alkyl substitutions on these substrates could easily enter and fully

occupy the binding pocket, but as the length of this substituent increases, the attached lactone group would be held farther from the catalytic dinuclear zinc center, for which a difference in k_{cat} values would be predicted. For example, C12-HSL actually has a K_M value 7-fold lower than that of C7-HSL, but catalysis is more significantly impaired, as seen in the 200-fold lower k_{cat} value. This selectivity mechanism is different from that used by other AHL lactonases characterized to date. However, we have shown that the nonhomologous, metal-independent N-terminal nucleophile hydrolase PvdQ uses a similar strategy to discriminate between N-acyl-HSL substrates of different lengths.⁴⁴

CONCLUSION

The quorum-quenching AHL lactonase from the potato root-associated *Chryseobacterium* sp. strain StRB126, AidC, has an unusually low K_M value for AHL substrates and displays a substrate selectivity stricter than that of any other related AHL lactonase characterized to date. At the time of writing, AidC also has the highest reported k_{cat}/K_M value for any characterized wild-type quorum-quenching enzyme, regardless of superfamily. Structural determination of AidC alone, and with bound product, reveals an unusual “kinked” helix and suggests a structural basis for the enhanced selectivity. Further studies will be required to determine how and if this selectivity impacts the chemical ecology of *Chryseobacterium* sp., but we note that *Erwinia carotovora*, a phytopathogen relevant to potatoes, produces AHLs within the optimal range for AidC substrates,⁴⁵ and that AHL lactonases have been shown to impact rhizosphere competence.⁴⁶ Intriguingly, AidC shows some structural similarities that more closely match families more distant from AHL lactonases, sharing a dimeric structure similar to that of an organic phosphotriesterase and an active-site histidine residue similar to that found in related phosphodiesterases. Tawfik and co-workers have identified an entirely different superfamily in which both paraoxonase and lactonase activities have evolved^{47–49} and may, by comparison, provide insight into the relationship of the various activities found in AHL lactonase homologues. AidC serves as an example for understanding how quorum-quenching enzymes can achieve selectivity between structurally similar AHL substrates and may serve as an efficient catalytic template amenable to further optimization for a broad array of quorum-quenching applications.

ASSOCIATED CONTENT

Supporting Information

Six figures comprised of protein and DNA coding sequences used for AidC expression (Figure S1), secondary structure assignment and topology diagram (Figure S2), graph of initial rates versus enzyme concentration (Figure S3), structure-based sequence alignment (Figure S4), LigPlot diagram of ligand–protein interactions (Figure S5), and a $2F_o - F_c$ omit map for the product-bound AidC complex. The Supporting Information is available free of charge on the ACS Publications website at DOI: 10.1021/acs.biochem.5b00499.

Accession Codes

Coordinates and structure factors have been submitted to the Protein Data Bank as entries 4ZO2 for AidC and 4ZO3 for AidC:C6-Hse.

AUTHOR INFORMATION

Corresponding Authors

*For correspondence regarding enzymology: University of Texas at Austin, 107 W. Dean Keeton St., Stop C0850, BME 6.202D, Austin, TX 78712-1081. Telephone: 512-232-4000. Fax: 512-232-2606. E-mail: walt.fast@austin.utexas.edu.

*For correspondence regarding X-ray structure determinations. Telephone: 773-508-3093. E-mail: dliu@luc.edu.

Author Contributions

R.M. (structure) and P.W.T. (enzymology) share first authorship.

Funding

This work was supported in part by National Science Foundation Grant CHE-1308672 (to W.F. and D.L.), the Robert A. Welch Foundation (Grant F-1572 to W.F.), Loyola University Chicago (to D.L.), and the National Institutes of Health (Grant GM111639 to Q.Q.H.). Results shown in this report are derived from work performed at Argonne National Laboratory, Structural Biology Center at the Advanced Photon Source. Argonne is operated by UChicago Argonne, LLC, for the U.S. Department of Energy, Office of Biological and Environmental Research, under Contract DE-AC02-06CH11357.

Notes

The authors declare no competing financial interest.

ACKNOWLEDGMENTS

We thank the Structural Biology Center (SBC) staff at ANL for help with data collection. We thank Mr. Haoming Jiang for assistance with the manuscript.

REFERENCES

- Schuster, M.; Sexton, D. J.; Diggle, S. P.; and Greenberg, E. P. (2013) Acyl-Homoserine Lactone Quorum Sensing: From Evolution to Application. *Annu. Rev. Microbiol.* 67, 43–63.
- Tay, S. B., and Yew, W. S. (2013) Development of quorum-based anti-virulence therapeutics targeting Gram-negative bacterial pathogens. *Int. J. Mol. Sci.* 14, 16570–16599.
- Amara, N.; Krom, B. P.; Kaufmann, G. F.; and Meijler, M. M. (2011) Macromolecular inhibition of quorum sensing: enzymes, antibodies, and beyond. *Chem. Rev.* 111, 195–208.
- Hong, K. W.; Koh, C. L.; Sam, C. K.; Yin, W. F.; and Chan, K. G. (2012) Quorum quenching revisited—from signal decays to signalling confusion. *Sensors* 12, 4661–4696.
- Kalia, V. C., and Purohit, H. J. (2011) Quenching the quorum sensing system: potential antibacterial drug targets. *Crit. Rev. Microbiol.* 37, 121–140.
- Romero, M.; Acuna, L.; and Otero, A. (2012) Patents on quorum quenching: interfering with bacterial communication as a strategy to fight infections. *Recent Pat. Biotechnol.* 6, 2–12.
- Zhu, J., and Kaufmann, G. F. (2013) Quo vadis quorum quenching? *Curr. Opin. Pharmacol.* 13, 688–698.
- Fast, W., and Tipton, P. A. (2012) The enzymes of bacterial census and censorship. *Trends Biochem. Sci.* 37, 7–14.
- Wang, W. Z.; Morohoshi, T.; Someya, N.; and Ikeda, T. (2012) AidC, a novel N-acylhomoserine lactonase from the potato root-associated *Cytophaga-Flavobacteria-Bacteroides* (CFB) group bacterium, *Chryseobacterium* sp. StRB126. *Appl. Environ. Microbiol.* 78, 7985–92.
- Pearson, W. R. (1990) Rapid and sensitive sequence comparison with FASTP and FASTA. *Methods Enzymol.* 183, 63–98.
- Dong, Y. H.; Xu, J. L.; Li, X. Z.; and Zhang, L. H. (2000) AiiA, an enzyme that inactivates the acylhomoserine lactone quorum-sensing signal and attenuates the virulence of *Erwinia carotovora*. *Proc. Natl. Acad. Sci. U. S. A.* 97, 3526–3531.

- (12) Carlier, A., Uroz, S., Smadja, B., Fray, R., Latour, X., Dessaux, Y., and Faure, D. (2003) The Ti plasmid of *Agrobacterium tumefaciens* harbors an attM-paralogous gene, *aiiB*, also encoding N-Acyl homoserine lactonase activity. *Appl. Environ. Microbiol.* 69, 4989–4993.
- (13) Liu, D., Momb, J., Thomas, P. W., Moulin, A., Petsko, G. A., Fast, W., and Ringe, D. (2008) Mechanism of the quorum-quenching lactonase (AiiA) from *Bacillus thuringiensis*. 1. Product-bound structures. *Biochemistry* 47, 7706–7714.
- (14) Momb, J., Wang, C., Liu, D., Thomas, P. W., Petsko, G. A., Guo, H., Ringe, D., and Fast, W. (2008) Mechanism of the quorum-quenching lactonase (AiiA) from *Bacillus thuringiensis*. 2. Substrate modeling and active site mutations. *Biochemistry* 47, 7715–7725.
- (15) Wang, L. H., Weng, L. X., Dong, Y. H., and Zhang, L. H. (2004) Specificity and enzyme kinetics of the quorum-quenching N-Acyl homoserine lactone lactonase (AHL-lactonase). *J. Biol. Chem.* 279, 13645–13651.
- (16) Liu, D., Thomas, P. W., Momb, J., Hoang, Q. Q., Petsko, G. A., Ringe, D., and Fast, W. (2007) Structure and specificity of a quorum-quenching lactonase (AiiB) from *Agrobacterium tumefaciens*. *Biochemistry* 46, 11789–11799.
- (17) Tang, K., Su, Y., Brackman, G., Cui, F., Zhang, Y., Shi, X., Coenye, T., and Zhang, X. H. (2015) MomL, a novel marine-derived N-acyl homoserine lactonase from *Muricauda olearia*. *Appl. Environ. Microbiol.* 81, 774–782.
- (18) Momb, J., Yoon, D. W., and Fast, W. (2010) Enzymic disruption of N-acyl-L-homoserine lactone-based quorum sensing. *ChemBioChem* 11, 1535–1537.
- (19) Thomas, P. W., and Fast, W. (2011) Heterologous over-expression, purification, and in vitro characterization of AHL lactonases. *Methods Mol. Biol.* 692, 275–290.
- (20) Gill, S. C., and von Hippel, P. H. (1989) Calculation of protein extinction coefficients from amino acid sequence data. *Anal. Biochem.* 182, 319–326.
- (21) Thomas, P. W., Zheng, M., Wu, S., Guo, H., Liu, D., Xu, D., and Fast, W. (2011) Characterization of purified New Delhi metallo-beta-lactamase-1. *Biochemistry* 50, 10102–10113.
- (22) Battye, T. G., Kontogiannis, L., Johnson, O., Powell, H. R., and AG, L. (2011) iMOSFLM: a new graphical interface for diffraction-image processing with MOSFLM. *Acta Crystallogr., Sect. D: Biol. Crystallogr.* 67, 27–81.
- (23) Collaborative Computational Project, No. 4 (1994) The CCP4 suite: Programs for protein crystallography. *Acta Crystallogr. D50*, 760–763.
- (24) Adams, P. D., Grosse-Kunstleve, R. W., Hung, L. W., Ioerger, T. R., McCoy, A. J., Moriarty, N. W., Read, R. J., Sacchettini, J. C., Sauter, N. K., and Terwilliger, T. C. (2002) PHENIX: building new software for automated crystallographic structure determination. *Acta Crystallogr., Sect. D: Biol. Crystallogr.* 58, 1948–1954.
- (25) Gotthard, G., Hiblot, J., Gonzalez, D., Elias, M., and Chabriere, E. (2013) Structural and enzymatic characterization of the phosphotriesterase OPHC2 from *Pseudomonas pseudoalcaligenes*. *PLoS One* 8, e77995.
- (26) Winn, M. D., Ballard, C. C., Cowtan, K. D., Dodson, E. J., Emsley, P., Evans, P. R., Keegan, R. M., Krissinel, E. B., Leslie, A. G., McCoy, A., McNicholas, S. J., Murshudov, G. N., Pannu, N. S., Potterton, E. A., Powell, H. R., Read, R. J., Vagin, A., and Wilson, K. S. (2011) Overview of the CCP4 suite and current developments. *Acta Crystallogr., Sect. D: Biol. Crystallogr.* 67, 235–242.
- (27) Emsley, P., and Cowtan, K. (2004) Coot: model-building tools for molecular graphics. *Acta Crystallogr., Sect. D: Biol. Crystallogr.* 60, 2126–2132.
- (28) Paettersen, E., Goddard, T., Huang, C., Couch, G., Greenblatt, D., Meng, E., and Ferrin, T. (2004) UCSF Chimera—a visualization system for exploratory research and analysis. *J. Comput. Chem.* 25, 1605–1612.
- (29) Liu, D., Lepore, B. W., Petsko, G. A., Thomas, P. W., Stone, E. M., Fast, W., and Ringe, D. (2005) Three-dimensional structure of the quorum-quenching N-acyl homoserine lactone hydrolase from *Bacillus thuringiensis*. *Proc. Natl. Acad. Sci. U. S. A.* 102, 11882–11887.
- (30) Eisenthal, R., Danson, M. J., and Hough, D. W. (2007) Catalytic efficiency and k_{cat}/K_M : a useful comparator? *Trends Biotechnol.* 25, 247–249.
- (31) Ahlgren, N. A., Harwood, C. S., Schaefer, A. L., Giraud, E., and Greenberg, E. P. (2011) Aryl-homoserine lactone quorum sensing in stem-nodulating photosynthetic bradyrhizobia. *Proc. Natl. Acad. Sci. U. S. A.* 108, 7183–7188.
- (32) Murzin, A. G., Brenner, S. E., Hubbard, T., and Chothia, C. (1995) SCOP: a structural classification of proteins database for the investigation of sequences and structures. *J. Mol. Biol.* 247, 536–540.
- (33) Kim, M. K., and Kang, Y. K. (1999) Positional preference of proline in alpha-helices. *Protein Sci.* 8, 1492–1499.
- (34) Barlow, D. J., and Thornton, J. M. (1988) Helix geometry in proteins. *J. Mol. Biol.* 201, 601–619.
- (35) Woolfson, D. N., and Williams, D. H. (1990) The influence of proline residues on alpha-helical structure. *FEBS Lett.* 277, 185–188.
- (36) Krissinel, E., and Henrick, K. (2007) Inference of macromolecular assemblies from crystalline state. *J. Mol. Biol.* 372, 774–797.
- (37) Holm, L., and Rosenstrom, P. (2010) Dali server: conservation mapping in 3D. *Nucleic Acids Res.* 38, W545–549.
- (38) Kostecky, B., Pohl, E., Vogel, A., Schilling, O., and Meyer-Klaucke, W. (2006) The crystal structure of the zinc phosphodiesterase from *Escherichia coli* provides insight into function and cooperativity of tRNase Z-family proteins. *J. Bacteriol.* 188, 1607–1614.
- (39) Crowder, M. W., Spencer, J., and Vila, A. J. (2006) Metallo-beta-lactamases: novel weaponry for antibiotic resistance in bacteria. *Acc. Chem. Res.* 39, 721–728.
- (40) Burgi, H. B., and Dunitz, J. D. (1983) From Crystal Statics to Chemical Dynamics. *Acc. Chem. Res.* 16, 153–161.
- (41) Minagawa, A., Takaku, H., Ishii, R., Takagi, M., Yokoyama, S., and Nashimoto, M. (2006) Identification by Mn^{2+} rescue of two residues essential for the proton transfer of tRNase Z catalysis. *Nucleic Acids Res.* 34, 3811–3818.
- (42) de la Sierra-Gallay, I. L., Pellegrini, O., and Condon, C. (2005) Structural basis for substrate binding, cleavage and allostery in the tRNA maturase RNase Z. *Nature* 433, 657–661.
- (43) Liu, C. F., Liu, D., Momb, J., Thomas, P. W., Lajoie, A., Petsko, G. A., Fast, W., and Ringe, D. (2013) A phenylalanine clamp controls substrate specificity in the quorum-quenching metallo-gamma-lactonase from *Bacillus thuringiensis*. *Biochemistry* 52, 1603–1610.
- (44) Clevenger, K. D., Wu, R., Liu, D., and Fast, W. (2014) n-Alkylboronic acid inhibitors reveal determinants of ligand specificity in the quorum-quenching and siderophore biosynthetic enzyme PvdQ. *Biochemistry* 53, 6679–6686.
- (45) Von Bodman, S. B., Bauer, W. D., and Coplin, D. L. (2003) Quorum sensing in plant-pathogenic bacteria. *Annu. Rev. Phytopathol.* 41, 455–482.
- (46) Park, S. J., Park, S. Y., Ryu, C. M., Park, S. H., and Lee, J. K. (2008) The role of AiiA, a quorum-quenching enzyme from *Bacillus thuringiensis*, on the rhizosphere competence. *J. Microbiol. Biotechnol.* 18, 1518–1521.
- (47) Afriat, L., Roodveldt, C., Manco, G., and Tawfik, D. S. (2006) The latent promiscuity of newly identified microbial lactonases is linked to a recently diverged phosphotriesterase. *Biochemistry* 45, 13677–13686.
- (48) Bar-Rogovsky, H., Hugenmatter, A., and Tawfik, D. S. (2013) The evolutionary origins of detoxifying enzymes: the mammalian serum paraoxonases (PONs) relate to bacterial homoserine lactonases. *J. Biol. Chem.* 288, 23914–23927.
- (49) Elias, M., and Tawfik, D. S. (2012) Divergence and convergence in enzyme evolution: parallel evolution of paraoxonases from quorum-quenching lactonases. *J. Biol. Chem.* 287, 11–20.
- (50) Clevenger, K. D., Wu, R., Er, J. A., Liu, D., and Fast, W. (2013) Rational design of a transition state analogue with picomolar affinity for *Pseudomonas aeruginosa* PvdQ, a siderophore biosynthetic enzyme. *ACS Chem. Biol.* 8, 2192–2200.

(51) Chow, J. Y., Wu, L., and Yew, W. S. (2009) Directed evolution of a quorum-quenching lactonase from *Mycobacterium avium* subsp. *paratuberculosis* K-10 in the amidohydrolase superfamily. *Biochemistry* 48, 4344–4353.

(52) Hiblot, J., Bzdrenga, J., Champion, C., Chabriere, E., and Elias, M. (2015) Crystal structure of VmoLac, a tentative quorum quenching lactonase from the extremophilic crenarchaeon *Vulcanisaeta moutnovskia*. *Sci. Rep.* 5, 8372.

(53) Chow, J. Y., Xue, B., Lee, K. H., Tung, A., Wu, L., Robinson, R. C., and Yew, W. S. (2010) Directed evolution of a thermostable quorum-quenching lactonase from the amidohydrolase superfamily. *J. Biol. Chem.* 285, 40911–40920.